Neurocomputing 228 (2017) 29–36

Contents lists available at ScienceDirect

Neurocomputing

journal homepage: www.elsevier.com/locate/neucom

Image splicing detection based on Markov features in QDCT domain☆

Ce Li[a,b,*], Qiang Ma[b], Limei Xiao[b], Ming Li[b], Aihua Zhang[b]

[a] School of Electronic and Information Engineering, Xian Jiaotong University, Xian 710049, China
[b] College of Electrical and Information Engineering, Lanzhou University of Technology, Lanzhou 730050, China

ARTICLE INFO

Keywords:
Markov model
Quaternion discrete cosine transform
Image splicing
Color image for detection

ABSTRACT

Image splicing is very common and fundamental in image tampering. Therefore, image splicing detection has attracted more and more attention recently in digital forensics. Gray images are used directly, or color images are converted to gray images before be processed in previous image splicing detection algorithms. However, most forgery images are color images. In order to make use of the color information in images, a classification algorithm is put forward which can use color images directly. In this paper, an algorithm based on Markov in quaternion discrete cosine transform (QDCT) domain is proposed for image splicing detection. First of all, color information is extracted from blocked images to construct quaternion in a whole manner, and the QDCT coefficients of quaternion blocked images can be obtained. Secondly, the expanded Markov features generated from the transition probability matrices in QDCT domain can not only capture the intra-block, but also the inter-block correlation between block QDCT coefficients. Finally, support vector machine (SVM) is exploited to classify the Markov feature vector. The experiment results demonstrate that the proposed algorithm not only make use of color information of images, but also can yield considerably better detection performance compared with the state-of-the-art splicing detection methods tested on the same dataset.

1. Introduction

In recent years, with the rapid development of mobile digital electronic technology and multimedia internet technology, human can easily use multimedia devices such as mobile phones, digital cameras to take pictures they expect. They also can use image processing software to edit pictures on computer optionally, to make the pictures can be spread in the Internet, which result in a problem that the content of original digital image has copyright is difficult to be protected. Recently, several of image tampering incidents happened [1], which threaten social justice and national security, hence, how to effectively identify the authenticity of images have been paid widely attention. Therefore, it is significant to develop some effective methods to detect tampering with the digital image.

As to the development of image processing technology [2], forensic technology also will be developed. Digital image authentication can be roughly divided into two categories, referred to as active [3] and passive [4], respectively. Compared with the active methods, an image can be authenticated by the passive ones that do not require prior information about the source image, which has attracted more and more attentions recently.

Although passive techniques need to depend on the concept of hypothesis, any trace may not be left in tampering images on the vision. In other words, the underlying statistics of tampering images are likely to be changed. Passive techniques are used these inconsistencies to detect the tampering. In image tampering, there are two common problems: copy-move tamper and image splicing tamper. For these two tamper technology, scholars put forward the corresponding detection methods, namely Copy-move detection and image splicing detection. The primary mission of copy-move detection is to detect whether two or more similar regions in a single image exist, and to locate them if there is any. The use of local visual features such as SIFT [4] for copy-move detection attracts much interest. Image splicing detection, on the contrary, aims at detecting whether a given image is synthesized from cutting and joining two or more pictures. In this paper, we mainly focus on the detection of digital image splicing forgery.

At the same time, image processing methods of quaternion discrete cosine transform have been applied to the color image registration [5], image saliency detection [6], and other fields. The superiority of QDCT in color image processing is fully reflected in these applications. But in the most of current image tamper detection algorithms, color image is converted to gray image before the image is processed, and the color

☆ Preliminary version of this manuscript has been selected in International Conference on Intelligent Computing (ICIC), 2015 (Paper ID: 510, Title:Image Splicing Detection Based on Markov Features in QDCT Domain) and its extended version is sub-selected for the Neurocomputing journal.

* Corresponding author at: School of Electronic and Information Engineering, Xian Jiaotong University, Xian 710049, China.
E-mail address: xjtulice@gmail.com (C. Li).

http://dx.doi.org/10.1016/j.neucom.2016.04.068
Received 24 December 2015; Received in revised form 13 March 2016; Accepted 10 April 2016
Available online 02 November 2016
0925-2312/

information are not taken into account. Images can be processed by quaternion in a whole manner and the color distortion can be avoided, thus the accuracy of the image tamper detection algorithm is improved. Meanwhile, the energy of spectral coefficient through QDCT is intensive with good property of eliminating redundancy, and QDCT is easy to quantitative analysis. Therefore, an image tamper detection algorithm under QDCT transform domain is put forward in this paper, new ideas for image tamper detection research are provided, and the algorithm has a certain theoretical and practical significance.

The remainder of paper is organized as Section 2 contains related work on splicing detection. Section 3 presents introduction to the proposed method. Section 4 is experiments and results. Section 5 is conclusion.

2. Related work

Image splicing forgery technique generally includes two categories. First one is a part of the image which is copied and pasted in another part of the same image to conceal an object or to duplicate certain image elements. Second one is merging two or more images together. Thus the original image is obviously changed to form a forged image. Supposing that different backgrounds of image are merged, it becomes difficult to perceive the changes of the borders and boundaries. As shown in Fig. 1, if there is no Fig. 1(a) and (b) as the standard reference, it's difficult to find Fig. 1(c) is spliced by two images from the front. Important traces are provided by presence of abrupt modification between different regions are combined and their backgrounds, so that splicing can be detected in the image.

For the past few years, various kinds of passive image splicing detection approaches have been proposed. Farid [7] exploited bispectral analysis to detect unnatural higher-order correlations into the signal by the forgery process, show their effectiveness in analyzing human speech. Quadratic phase coupling was used in detection algorithm of natural images and splicing images by Ng and Chang S-F who works in Columbia University, success rate was 72% [8]. For this work, they created a data set [9]. In New Jersey Institute of Technology, the basis of the model of natural images, 266-d feature vector consist of Wavelet moment characteristics and Markov features was used to identify splicing images by Shi *et al.* success rate was 91.8% [10] on columbia image splicing detection evaluation dataset [9]. The advantage of this method is the low dimension of feature vectors, and can acquire high accuracy.

Wang et al. [11] proposed a method for splicing detection for color images using gray level co-occurrence matrix (GLCM) in Institute of Automation Chinese Academy of Sciences. GLCM of the threshold edge image was used. In literature [12], the edge image of image chroma component was modeled as a finite-state Markov chain and low dimensional feature vector was extracted from its stationary distribution for tampering detection. The detection accuracy of 95.6% was achieved on their own constructed Image Splicing Detection Evaluation Dataset (CASIA TIDE V2.0) [13]. Sutthiwan et al. [14] had pointed out two problems of the database [13] and shown how to rectify the CASIA TIDE V2.0 dataset, their experimental results showed that the detection rate of the causal Markov model based features was reduced to 78% on the rectified dataset.

Recently, most of the methods [15–18] are based on the Markov features, because the Markov transition probability features can reveal the dependencies between adjacent pixels when there is a change due to splicing. A 2-D noncausal Markov model was proposed by Zhao et al. [15] in the block discrete cosine transformation domain and the discrete Meyer wavelet transform domain, a higher detection rate was achieved. A tamper detection algorithm of natural images and splicing images was proposed by Huang et al. in Sun Yat sen University, their method used Markov features in DCT and DWT domain, and the precision of detection was up to 93.42% [16] on columbia image splicing detection evaluation dataset [9]. They achieved detection accuracy of 89.76% on image splicing detection evaluation dataset (CASIA TIDE V2.0) [13]. The weaknesses of this method is the high dimension of feature vectors, and can consume much time to extract feature vectors.

Like other algorithms, we will also make image Splicing problem as a pattern recognition problem, in other words we make this problem as a binary classification problem. Pattern recognition in many ways [19,20], because of the nature of SVM has a good sample, nonlinear nature, these advantages it is suitable for classification of the problem, so we chose SVM as the classifier. Because these algorithms mainly use the gray information of images or certain color component information to detect whether the images have been spliced, the whole color information is not used effectively. In order to make full use of the color information, QDCT is introduced into image splicing detection algorithm in this paper. QDCT was put forward by Feng Wei and Hu Bo [5] in 2008, the calculation was given and the application of QDCT in color template matching was analyzed. A detection algorithm of image saliency based on QDCT was proposed by Schauerte et al. [6] in 2012. Therefore, an image tamper detection method in QDCT domain is proposed in this paper. This new idea has a certain theoretical significance.

3. The proposed approach

In this section, the whole frame work of the proposed algorithm is presented, followed by detailed description of each part.

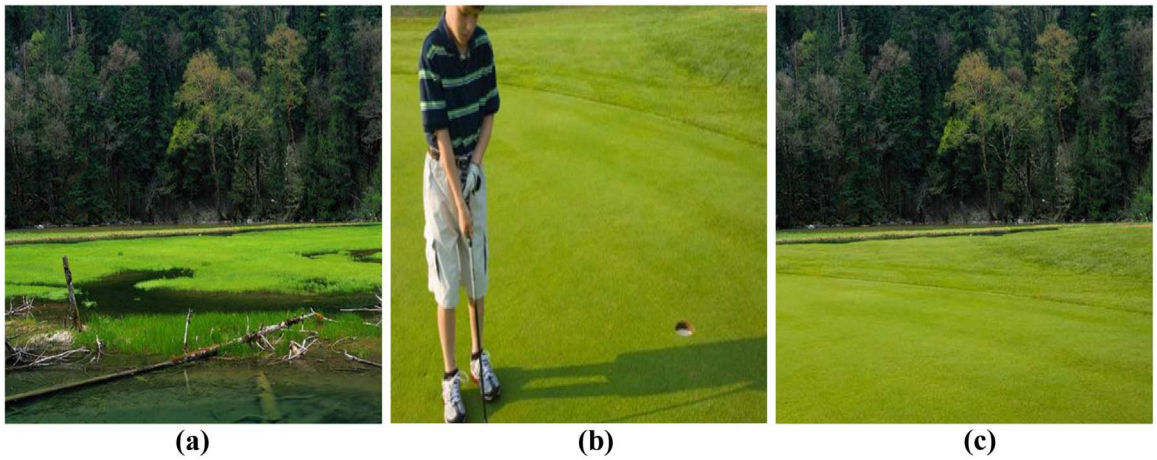

Fig. 1. Multi-image splicing image tampering sample.(a) source image 1, (b) source image 2, (c) splicing image.

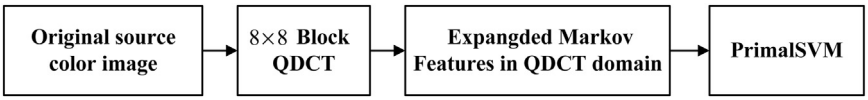

Fig. 2. Illustration of the stages of our algorithm.

3.1. Algorithm framework

The framework of the proposed approach based on Markov features is shown in Fig. 2. Compared with literature [16], we extract Markov features in QDCT domain. Expanded Markov features in QDCT domain are obtained in this paper. Compared with [10], we introduce main diagonal difference matrices, minor diagonal difference matrices, main diagonal transition probability matrices and minor diagonal transition probability matrices in QDCT. Different the literature [10,16], we also consider QDCT coefficients correlation between the intra-block correlation and the inter-block in main diagonal and minor diagonal direction. First of all, color information is extracted from blocked images to construct quaternion and apply QDCT with it, thus the QDCT coefficients of blocked images can be obtained. Secondly, the expanded Markov features generated from the transition probability matrices in QDCT domain can not only capture the intra-block, but also the inter-block correlation between block QDCT coefficients. Finally, the feature vector obtained is used to distinguish authentic and spliced images with Primal SVM [21] as the classifier.

3.2. Quaternion discrete cosine transform

3.2.1. Definition and operational rule of quaternion

Quaternion could be regarded as the generalization of complex number, it includes a real part component and several imaginary part components, such as Quaternion, Octonion, Sedenion and so on. Quaternion is one of the most common and simple expression, the definition and some basic operation properties are introduced as follows:

(1) The definition of quaternion

$$q = w + xi + yj + zk \tag{1}$$

Here w, x, y, z are real number, i, j and k are operators of complex number and vector, they all satisfy Hamilton rule:

$$j = k, jk = i, ki = jji = -k, kj = -i, ik = -j$$

And they also satisfy $i^2 = j^2 = k^2 = ijk = -1$, but they do not satisfy commutative property of multiplication. The conjugate of quaternion is $\bar{q} = w - xi - yj - zk$ the module is:

$$|q| = \sqrt{w^2 + x^2 + y^2 + z^2} \tag{2}$$

Here, the quaternion with zero real part is pure quaternion, and the quaternion with unit module is called unit quaternion.

(2) Plural expression of quaternion.

Clay-Dickson theorem [22] has indicated how to construct a quaternion by two complex numbers, suppose $m, n \in C$, $m = w + xi$, $n = y + zi$, $w, x, y, z \in R$, then

$$q = m + nj, q \in Q, j^2 = -1 \tag{3}$$

Thus,

$$q = w + xi + (y + zi)j \quad = w + xi + yj + zij \quad = w + xi + yj + zk$$

The transformation above show the process of establishing quaternion by complex numbers, and the quaternion can be called the complex number of complex number or hypercomplex number. i, j, k are three mutually perpendicular axes, from Hamilton rule, the relationship between them are obtained and right-handed rule is also satisfied.

In some calculations, quaternion is not always decomposed according to the directions of i, j strictly, which requires a unit pure imaginary quaternion coordinate axis of isomorphic i, j axes need to be constructed when quaternion is processed. Suppose that axes of the two unit pure imaginary quaternion are μ_1, μ_2 respectively, and they satisfy $\mu_1 \perp \mu_2$, then q can be decomposed one complex coordinate at the direction μ_1, and q can also be decomposed another complex coordinate at the direction μ_2.

$$q = m' + n'\mu_2, x \in Q, \mu_2^2 = -1 \tag{4}$$

Where, $m' = w' + x'\mu_1, n' = y' + z'\mu_1, w', x', y', z' \in R$ then $q = w' + x'\mu_1 + y'\mu_2 + z'\mu_3$. Here, $\mu_3 = \mu_1\mu_2$, and $\mu_3 \perp \mu_1$, $\mu_3 \perp \mu_2$.

A series of transformation above are similar to planimetric coordinate transformation, but the coordinate is expressed from the perspective of three imaginary numbers basis of quaternion: the coordinate (x, y, z) under i, j, k is transformed into the coordinate (w', x', y', z') under μ_1, μ_2, μ_3. The transformation will be applied in the realization of DWT.

3.2.2. Quaternion discrete cosine transform

In the field of real number and the field of complex number, concentration degree of energy of inputing information through two-dimensional discrete cosine transform (DCT) is higher than the inputting information's after DFT transform. The inputing information can be got approximatively by inverse transformation of several main coefficients (also known as pivot elements) after two-dimensional DCT.

The research of QDCT is prompted by the precedents of the successful application of real number and complex number domain, the basic principle of QDCT was proposed by Feng and Hu [5], and the actual algorithm was given.

$h_q(m, n)$ is a two-dimensional $M \times N$ quaternion matrix, m and n is row and column of the matrix respectively, here, $m \in [0, M-1]$, $n \in [0, N-1]$, the definition of L-QDCT and R-QDCT are as follows:

L-QDCT:

$$J_q^L(p, s) = \alpha(p)\alpha(s) \sum_{m=0}^{M-1} \sum_{n=0}^{N-1} u_q \cdot h_q(m, n) \cdot T(p, s, m, n) \tag{5}$$

R-QDCT:

$$J_q^R(p, s) = \alpha(p)\alpha(s) \sum_{m=0}^{M-1} \sum_{n=0}^{N-1} h_q(m, n) \cdot T(p, s, m, n) \cdot u_q \tag{6}$$

In formula (5) and (6), u_q is a unit pure quaternion, it can represent the direction of axis of transformation, and it satisfies $u_q^2 = -1$, p and s is row and column of the transform matrix respectively. it is similar to DCT in real number and complex number domain the definition of $\alpha(p)$, $\alpha(s)$ and $T(p, s, m, n)$ are as follows:

$$\alpha(p) = \begin{cases} \sqrt{1/M} & p = 0 \\ \sqrt{2/M} & p \neq 0, \end{cases} \quad \alpha(s) = \begin{cases} \sqrt{1/N} & s = 0 \\ \sqrt{2/N} & s \neq 0. \end{cases} T(p, s, m,$$

$$n) = \cos\left[\frac{\pi(2m+1)p}{2M}\right] \cos\left[\frac{\pi(2n+1)s}{2N}\right]$$

The spectral coefficient of $J(p, s)$ through transformation is still a quaternion matrix of $M \times N$, and its representation is by formula (7).

$$J(p, s) = J_0(p, s) + J_1(p, s)i + J_2(p, s)j + J_3(p, s)k \tag{7}$$

In our algorithm, we chose L-QDCT to do block QDCT. The realization of QDCT transform: the computational complexity of QDCT transform can be seen from its definition, in order to avoid wasting of resources resulted from complicated calculation, the approach of QDCT is designed on the basis of DCT that is widely used in the field of real number and complex number, the steps are as follows (take L-QDCT as

an example):

(a) For a given quaternion matrix $h(m, n)$, transform it into Cayley-Dickson form: $h(m, n) = h_{\|}(m, n) + h_{\perp}(m, n)u_2$, decompose it into a specified axis, here, $h_{\|}(m, n)$ and $h_{\perp}(m, n)$ are complex matrices;.

(b) According to Clay-Dickson theorem, convert $h_{\|}(m, n)$ and $h_{\perp}(m, n)$ under the coordinate u_1 into $h_a(m, n)$ and $h_b(m, n)$ under the coordinate i, thus $h'(m, n) = h_a(m, n) + h_b(m, n)j$;.

(c) Calculate the discrete cosine of standard complex number domain of $h_a(m, n)$ and $h_b(m, n)$ to obtain $J_a(p, s)$ and $J_b(p, s)$, then obtain $J'(p, s) = J_a(p, s) + J_b(p, s)j$;.

(d) Multiply $J'(p, s)$ and original axis to obtain QDCT, that is $J(p, s) = u_q \cdot J'(p, s)$, here, u_q is a unit pure quaternion of u_1, u_2, u_3.

3.3. Block QDCT

The Expanded Markov features in DCT domain proposed in [16] are very remarkable in capturing the differences between authentic and spliced images. They can be calculated by seven steps.

Unlike the first step, the original color images are blocked into 8×8 non-repeatedly, and each block is still color image. Secondly, three color components of R, G and B of blocked images are utilized to construct quaternion matrix, and the quaternion matrix is processed by QDCT transform to obtain QDCT coefficient matrix of each block, then the real part(r) and three imaginary parts (i, j, k) of the square root of the four parts are calculated. Finally, all calculated matrices need to reassemble according to the site of blocking, thus a 8×8 blocked QDCT matrix F of original color image can be acquired. It is shown in Fig. 3.

3.4. Expanded Markov features in QDCT domain

Compared with the literature [16], expanded Markov features in QDCT domains are obtained in this paper. Besides, reference [10], we introduce main diagonal difference matrices, minor diagonal difference matrices, main diagonal transition probability matrices and minor diagonal transition probability matrices in QDCT. Different with the literature [10,16], we also consider QDCT coefficients correlation between intra-block correlation and inter-block in main diagonal and minor diagonal direction. Except this different, other steps are roughly the same. The following steps are shown.

Firstly, apply 8×8 block QDCT on the original image pixel array following Part 3.3, and the corresponding QDCT coefficient array A is obtained.

Secondly, we are round the QDCT coefficients A to integer and take absolute value (denote the obtained arrays F).

Thirdly, calculate the horizontal, vertical, main diagonal and minor diagonal intra-block difference 2-D arrays F_h, F_v, F_d and F_{-d} by applying Eqs. (8) to (11).

$$F_h(u, v) = F(u, v) - F(u + 1, v) \tag{8}$$

$$F_v(u, v) = F(u, v) - F(u, v + 1) \tag{9}$$

$$F_d(u, v) = F(u, v) - F(u + 1, v + 1) \tag{10}$$

$$F_{-d}(u, v) = F(u + 1, v) - F(u, v + 1) \tag{11}$$

and calculate the horizontal, vertical, main diagonal and minor diagonal inter-block difference 2-D arrays G_h, G_v, G_d and G_{-d} by applying Eqs. (12) to (15).

$$G_h(u, v) = F(u, v) - F(u + 8, v) \tag{12}$$

$$G_v(u, v) = F(u, v) - F(u, v + 8) \tag{13}$$

$$G_d(u, v) = F(u, v) - F(u + 8, v + 8) \tag{14}$$

$$G_{-d}(u, v) = F(u + 8, v) - F(u, v + 8) \tag{15}$$

Fourthly, introduce a threshold T ($T \in N_+$), if the value of an element in F_h(or F_v, F_d, F_{-d}, G_h, G_v, G_d and G_{-d}) is either greater than T or smaller than $-T$, replace it with T or $-T$, respectively, applying Eqs. (16).

$$a_{new} = \begin{cases} T, & a_{old} \geq T \\ -T, & a_{old} \leq T \\ a_{old}, & otherwise. \end{cases} \tag{16}$$

Fifthly, calculate the horizontal, vertical, main diagonal and minor diagonal transition probability matrices of F_h, F_v, F_d, F_{-d}, G_h, G_v, G_d and G_{-d} by applying Eqs. (17) to (28).

$$P1_h(i, j) = \frac{\sum_{u=1}^{S_u-2} \sum_{v=1}^{S_v} \delta(F_h(u, v) = i, F_h(u + 1, v) = j)}{\sum_{u=1}^{S_u} \sum_{v=1}^{S_v} \delta(F_h(u, v) = i)} \tag{17}$$

$$P1_v(i, j) = \frac{\sum_{u=1}^{S_u-1} \sum_{v=1}^{S_v-1} \delta(F_h(u, v) = i, F_h(u, v + 1) = j)}{\sum_{u=1}^{S_u-1} \sum_{v=1}^{S_v-1} \delta(F_h(u, v) = i)} \tag{18}$$

$$P2_h(i, j) = \frac{\sum_{u=1}^{S_u-1} \sum_{v=1}^{S_v-1} \delta(F_v(u, v) = i, F_v(u + 1, v) = j)}{\sum_{u=1}^{S_u-1} \sum_{v=1}^{S_v-1} \delta(F_v(u, v) = i)} \tag{19}$$

$$P2_v(i, j) = \frac{\sum_{u=1}^{S_u-1} \sum_{v=1}^{S_v-1} \delta(F_v(u, v) = i, F_v(u, v + 1) = j)}{\sum_{u=1}^{S_u-1} \sum_{v=1}^{S_v-1} \delta(F_v(u, v) = i)} \tag{20}$$

$$P1_d(i, j) = \frac{\sum_{u=1}^{S_u-2} \sum_{v=1}^{S_v-2} \delta(F_d(u, v) = i, F_d(u + 1, v + 1) = j)}{\sum_{u=1}^{S_u-2} \sum_{v=1}^{S_v-2} \delta(F_d(u, v) = i)} \tag{21}$$

$$P1_{-d}(i, j) = \frac{\sum_{u=1}^{S_u-2} \sum_{v=1}^{S_v-2} \delta(F_{-d}(u + 1, v) = i, F_{-d}(u, v + 1) = j)}{\sum_{u=1}^{S_u-2} \sum_{v=1}^{S_v-2} \delta(F_{-d}(u, v) = i)} \tag{22}$$

$$P3_h(i, j) = \frac{\sum_{u=1}^{S_u-16} \sum_{v=1}^{S_v} \delta(G_h(u, v) = i, G_h(u + 8, v) = j)}{\sum_{u=1}^{S_u-16} \sum_{v=1}^{S_v} \delta(G_h(u, v) = i)} \tag{23}$$

$$P3_v(i, j) = \frac{\sum_{u=1}^{S_u-8} \sum_{v=1}^{S_v-8} \delta(G_h(u, v) = i, G_h(u, v + 8) = j)}{\sum_{u=1}^{S_u-8} \sum_{v=1}^{S_v-8} \delta(G_h(u, v) = i)} \tag{24}$$

$$P4_h(i, j) = \frac{\sum_{u=1}^{S_u-8} \sum_{v=1}^{S_v-8} \delta(G_v(u, v) = i, G_v(u + 8, v) = j)}{\sum_{u=1}^{S_u-8} \sum_{v=1}^{S_v-8} \delta(G_v(u, v) = i)} \tag{25}$$

$$P4_v(i, j) = \frac{\sum_{u=1}^{S_u} \sum_{v=1}^{S_v-16} \delta(G_v(u, v) = i, G_v(u, v + 8) = j)}{\sum_{u=1}^{S_u} \sum_{v=1}^{S_v-16} \delta(G_v(u, v) = i)} \tag{26}$$

$$P3_d(i, j) = \frac{\sum_{u=1}^{S_u-16} \sum_{v=1}^{S_v-16} \delta(G_d(u, v) = i, G_d(u + 8, v + 8) = j)}{\sum_{u=1}^{S_u-16} \sum_{v=1}^{S_v-16} \delta(G_d(u, v) = i)} \tag{27}$$

$$P3_{-d}(i, j) = \frac{\sum_{u=1}^{S_u-16} \sum_{v=1}^{S_v-16} \delta(G_{-d}(u + 8, v) = i, G_{-d}(u, v + 8) = j)}{\sum_{u=1}^{S_u-16} \sum_{v=1}^{S_v-16} \delta(G_{-d}(u, v) = i)} \tag{28}$$

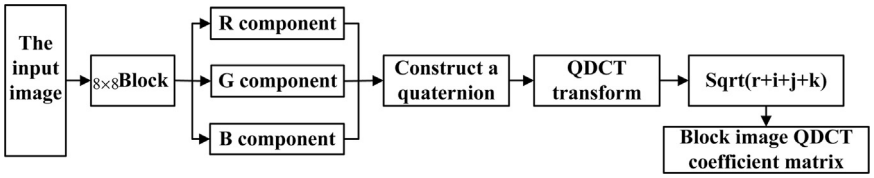

Fig. 3. Illustration of the stages of 8×8 Block QDCT.

Fig. 4. Some example images of CASIA TIDE V2.0 dataset (authentic images in the top row, their forgery counter parts in the bottom row).

Fig. 5. Some example images of CASIA TIDE V2.0 dataset (authentic images in the top and middle row, their forgery counter parts in the bottom row).

where $i, j \in \{-T, -T+1, \ldots, 0, \ldots T-1, T\}$, s_u and s_v denote the dimensions of the original source image. $\delta(\cdot) = 1$ if and only if its arguments are satisfied, otherwise $\delta(\cdot) = 0$. Thus $(2T+1) \times (2T+1) \times 12$ dimensionality Markov features in QDCT domain are obtained.

4. Experiments and results

In this section, we introduce the experiment image datasets at first, and then present a set of experiments to demonstrate the high performance and effectiveness of the proposed algorithm.

Table 1
Classification results of the proposed algorithm with different threshold T on CASIA TIDE V1.0 dataset.

Threshold T	Dimensionality n	TP (%)	TN (%)	Accuracy (%)
3	588	95.881	95.073	95.478
4	972	95.440	96.470	95.958
5	1452	95.735	97.131	96.435

Table 2
Classification results of the proposed algorithm with different threshold T on CASIA TIDE V2.0 dataset.

Threshold T	Dimensionality n	TP (%)	TN (%)	Accuracy (%)
3	588	88.371	95.637	92.003
4	972	89.185	95.567	92.377
5	1452	89.426	95.914	92.668

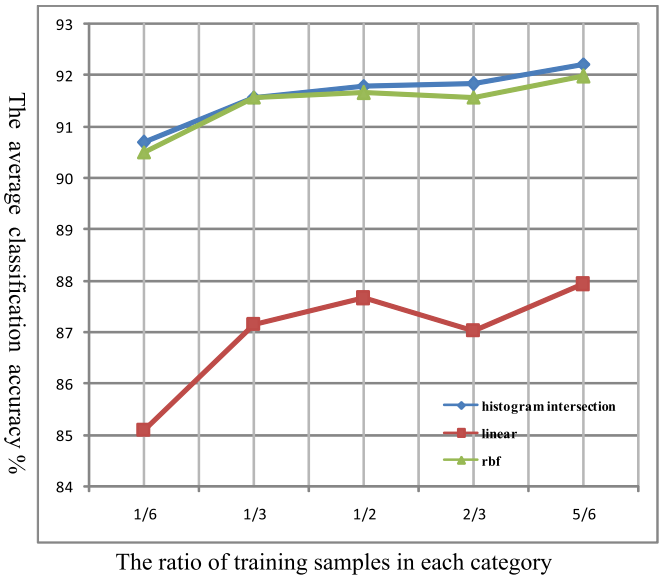

Fig. 6. The accuracy of different kernel functions.

Table 3
Classification results of the proposed algorithm without main diagonal and minor diagonal transition probability matrices on CASIA TIDE V1.0 dataset.

Threshold T	Dimensionality n	TP (%)	TN (%)	Accuracy (%)
3	392	92.648	90.810	91.727
4	648	93.825	92.647	93.236
5	968	94.854	95.581	95.217

Table 4
Experiment results obtained on CASIA TIDE V2.0 dataset.

Feature vector	NIM[10]	He[16]	Our method
Dimensionality	266	100	972
Accuracy (%)	84.86	89.76	92.38
Feature extraction time (s)	4.479	2.218	4.61
Feature selection time (s)	0	2.158	0
Total time (s)	4.479	4.376	4.61

4.1. Image dataset

Two available public image datasets for tampering detection, especially for splicing detection, are provided by DVMM, Columbia University [9]. The color information is not provided by their data of gray images, the amount of data of color images dataset is few, and doesn't have reality. In order to provide a more realistic and challenging evaluation database for image tampering detection, two color image datasets which is constructed by Institute of Automation Chinese Academy of Sciences are chosen to test our proposed approach. They are CASIA TIDE V1.0 (the CASIA image tempering detection evaluation database V1.0) and CASIA TIDE V2.0 (the CASIA image tempering detection evaluation database V2.0).

CASIA TIDE V1.0 is focus on splicing detection evaluation. Image splicing is de-fined as a simple cut-and-paste operation of image regions from one image to the same or another image without performing post-processing, which is a fundamental operation of tampering. CASIA TIDE V1.0 dataset contains 800 authentic images and 921 spliced color images of size 384×256 pixels with JPEG format. The authentic images are mostly collected from the Corel image dataset and others are taken by the authors digital cameras. V2.0 is upgrade of V1.0, so we only give some pictures examples of V2.0 dataset.

Compared to CASIA TIDE V1.0, CASIA TIDE V2.0 is with larger size and with more realistic and challenged fake images by using post-processing of tampered regions. It contains 7491 authentic and 5123 tampered color images. The images in CASIA TIDE V2.0 are with difference size, various from 240×160 to 900×600 pix-els. Unlike CASIA TIDE V1.0, CASIA TIDE V2.0 concludes uncompressed images and also JPEG images with different Q factors. The author added an extra indoor category to consider the impact of image illumination and consider post-processing of (boundary of) spliced regions. Some examples of CASAI TIDE V2.0 are shown in Figs. 4 and 5. Fig. 4 shows some example of single image splicing. Fig. 5 shows some example of multi-image splicing. As can be seen from these examples, splicing images are similar with nature images, so it brought a great challenge to classify splicing images nature images.

The two problems of the dataset CASAI TIDE V1.0 and CASAI TIDE V2.0 have been pointed out by Patchara et al. [14]. First one is the JPEG compression applied to authentic images is one-time less than that applied to tampered images; the second one is for JPEG images, the size of chrominance components of 7,140 authentic images is only one quarter of that of 2,061 tampered images. For fairness purpose, We according to the processing method to modify the database in the article [14]. However, the Ycbcr color space can not be used, so we just only need to solve the the first problem of CASAI TIDE V2.0. we used Matlab for standard JPEG compression to lessen the influence of the difference in the number of JPEG compressions by the following procedure: (1)Re-compressing 7,437 JPEG authentic images with quality factor=84; (2) Compressing 3,059 TIFF tampered images by Matlab with quality factor=84; (3)Leaving 2,064 JPEG tampered images untouched. The database CASAI TIDE V1.0 as well.

4.2. Classification

There are many classification methods of binary classification problem, such as clustering methods [23], support vector machine(SVM) methods, deep learning and so on. While simultaneously maximizing the geometric margin between two different classes, SVM can minimize the empirical classification error. In our experiment we chose PrimalSVM [19] to classification. The PrimalSVM have more kernel function, such as rbf, liner, histogram intersection and so on. After the comparison with several experiments, the histogram intersection kernel have the highest classification accuracy. Therefore, histogram intersection is chosen as kernel function. To be fair, we chose the threshold T same as other. For CASIA TIDE V1.0, CASIA TIDE V2.0 dataset, we chose T=4, then it will produce 972-dimensional feature vector.

In order to evaluate the performance of the proposed algorithm, all the experiments and comparisons are tested on the dataset mentioned above and the same classifier. The testing platform is Matlab R2012b, and the hardware platform is a PC with a 2 G core i3 processor. In each

experiment, the average rate of 20 repeating independent tests is recorded. In each of the 50 runs, 5/6 of the authentic images are randomly select and the SVM classifier is trained to 5/6 of the spliced images in the dataset. Then the remaining 1/6 of the authentic and spliced images are used to test the trained classifier.

4.3. The detection performance of the proposed approach

Some common experiments are conducted first to assess the detection ability of the proposed algorithm. The detailed results are shown in Tables 2, 3. Here, TP(true positive) rate is the ratio of correct classification of authentic images. TN (true negative) rate is the ratio of correct classification of spliced images. Accuracy of detection is the weighted average value of TP rate and TN rate.

4.3.1. Choice of threshold T

Another issue is the choice of the threshold T, which is used to reduce the Markov features dimensionality. To select an appropriate T, the following points should be taken into account. The T cannot be too small. If T is too small, the artifacts caused by splicing will not be able to be catched by the elements of the transition probability matrix sensitively. On the other hand, this T cannot be too large. If T is too large, the dimensionality of the transition probability matrix will be too large, which makes the computational complexity non-manageable, hence losing the meaning of using thresholding technique.

In Tables 1 and 2 we provide the performance of Markov features with three different T.

4.3.2. The contribution of diagonal transition probability matrices

In our algorithm, we not only considered horizontal and vertical transition probability matrices, but also considered main diagonal and minor diagonal transition probability matrices. In this section we will discuss how much the contribution of main diagonal and minor diagonal transition probability matrices for the classification accuracy. Through the comparison of Tables 1, 3, we can acquire a conclusion that main diagonal and minor diagonal transition probability matrices will improve nature and splicing image classification accuracy.

4.3.3. Choice of kernel function

Evaluation results obtained from the average classification accuracy of five times random training and testing. As shown in Fig. 6, we can see that with the ratio of images in each training sample increase from 1/6 to 5/6, the average accuracy with all kernels is improved, but the histogram intersection kernel have the highest classification accuracy. Therefore, we choose histogram intersection as kernel function, the ratio of training samples fixed at 5/6.

4.3.4. Comparison with other algorithms

To evaluate the proposed algorithm comprehensively, a comparison between the proposed algorithm and some state-of-the-art image splicing detection methods should be done. To ensure the validity and fairness of the reported results of different methods, all the comparison experiments are conducted in the same experimental setup described in Section 4.2, 4.3.1 and 4.3.2 The results of the experiments are shown in Table 3 (the feature vectors proposed in [10,16] are denoted as NIM and He respectively). Table 4 shows that the proposed algorithm outperforms other two presented splicing detection schemes. As far as we know, the detection accuracy 92.38% achieved by the proposed algorithm is the highest one having been attained on the CASIA TIDE V2.0 Dataset. The algorithms of NIM and Huang was firstly converted color image to gray image and extracted Markov features from DCT and DWT coefficients of gray image. Our algorithm is directly extracted Markov features from QDCT coefficients of image and obtained a higher accuracy than their algorithms. This was showed that our algorithm has more practical value.

5. Conclusion

In the most of current image tamper detection algorithms, color image is converted to gray image before the image is processed, and the color information are not taken into account. In our method, images can be processed by quaternion in a whole manner and the color distortion can be avoided, thus the accuracy of the image tamper detection algorithm is improved. Meanwhile, the energy of spectral coefficient through QDCT is intensive with good property of eliminating redundancy, and QDCT is easy to quantitative analysis. Therefore, a image tamper detection algorithm under QDCT transform domain is put forward in this paper, an algorithm based on Markov in QDCT domain is proposed for image splicing detection. The essence of the proposed method is blind detection of color image change by extending the Markov transition probability characteristics features from QDCT frequency domains to reveal the dependencies between adjacent pixels when there is a change due to splicing. The experiment results demonstrate that the proposed algorithm not only make use of color information of images, but also can significantly lead to improving the tampering detection rate, with more than 92.38% accuracy, as compared with the state-of-the-art splicing detection methods tested on the same dataset. Because the tamper images are mostly color in real life, this new idea for image tamper detection research has a certain theoretical and more practical significance.

Acknowledgments

The paper was supported in part by the National Natural Science Foundation (NSFC) of China under Grant No. (61365003,61302116), Gansu Province Basic Research Innovation Group Project (1506RJIA031), Natural Science Foundation of China in Gansu Province Grant No. 1308RJZA274, and China Postdoctoral Science Foundation (2014M550494).

References

[1] The website of Some image tampering incidents. ⟨http://hoaxes.org/photo_database/chronological/P110⟩.
[2] Xiao-Feng Wang, D.S. Huang, Huan Xu, An efficient local Chan-Vese model for image segmentation, Pattern Recognit. 43 (3) (2010) 603–618.
[3] Matthew, Holliman, Nasir Memon, Counterfeiting attacks on oblivious block-wise independent invisible watermarking schemes, IEEE Trans. Image Process. 9 (3) (2000) 432–441.
[4] I. Amerini, L. Ballan, R. Caldelli, A. Del Bimbo, G. Serra, A sift-based forensic method for copy move attack detection and transformation recovery, IEEE Trans. Inf. Forensics Secur. 6 (3) (2011) 1099–1110.
[5] Feng Wei, Hu Bo, Quaternion discrete cosine transform and its application in color template matching, IEEE Congr. Image Signal Process. 5 (2) (2008) 252–256.
[6] Schauerte Boris, Rainer Stiefelhagen, Quaternion-based Spectral Saliency Detection for Eye Fix-ation Prediction, European Conference on Computer Vision, 2012; pp. 116–129.
[7] Farid Hany, Detecting Digital Forgeries Using Bispectral Analysis, Technical Report, Mas-sachusetts Institute of Technology, 1999.
[8] T.-T. Ng, S.-F. Chang, Blind Detection of Digital Photomontage using Higher Order Sta-tistics, Technical Report 201-2004-1,Columbia University, 2004.
[9] T.-T. Ng, S.-F. Chang, Q. Sun, A Data Set of Authentic and Spliced Image Blocks, Columbia University, 2004.
[10] Shi Yun Q, Chunhua Chen, Wen Chen, A Natural Image Model Approach to Splicing Detection, ACM Proceedings of The 9th Workshop on Multimedia & Security, 2007; pp. 51–62.
[11] Wei Wang, Jing Dong, Tieniu Tan, Effective Image Splicing Detection Based on Image Chroma, IEEE International Conference on Image Processing, 2009; pp. 1257–1260.
[12] Wei Wang, Jing Dong, Tieniu Tan, Image Tampering Detection Based on Stationary Distribution of Markov Chain, IEEE International Conference on Image Processing, 2010; pp. 2101–2104.
[13] The CASIA TIDE dataset. ⟨http://forensics.idealtest.org/⟩
[14] Patchara Sutthiwan, Yun Q. Shi, Hong Zhao, Tian-Tsong Ng, Wei Su, Markovian Rake Transform for Digital Image Tampering Detection, Transactions on data hiding and multimedia security VI. Springer Berlin Heidelberg, 2011; pp. 1–17.
[15] Zhao Xudong, Wang Shilin, Li, Shenghong, Li Jianhua, Passive image-splicing detection by a 2-d noncausal markov model, IEEE Trans. Circuits Syst. Video Technol. 25 (2) (2015) 185–199.
[16] Zhongwei He, Wei Lu, Wei Sun, Jiwu, Huang digital image splicing detection based on markov features in DCT and DWT domain, Pattern Recognit. 45 (12) (2012)

4292–4299.
[17] El-Alfy, M. E-Sayed, Muhammad Ali Qureshi, Combining spatial and DCT based Markov features for enhanced blind detection of image splicing, Pattern Anal. Appl. 18 (3) (2015) 713–723.
[18] Hashmi, Mohammad Farukh, Avinash G. Keskar, Image forgery authentication and classification using hybridization of hmm and svm classifier, Int. J. Secur. Its Appl. 9 (4) (2015) 125–140.
[19] Zhong-Qiu Zhao, D.S. Huang, Bing-Yu. Sun, Human face recognition based on multiple features using neural networks committee, Pattern Recognit. Lett. 25 (12) (2004) 1351–1358.
[20] Li Shang, D.S. Huang, Ji-Xiang Du, Chun-Hou Zheng, Palmprint recognition using FastICA algorithm and radial basis probabilistic neural network, Neurocomputing 69 (13–15) (2006) 1782–1786.
[21] Chapelle, Olivier, Training A support vetor machine in the primal, Neural Comput. 19 (5) (2007) 1155–1178.
[22] Moxey C. Eddie, J. Stephen, Sangwine, Hypercomplex correlation techniques for vector images, IEEE Trans. Signal Process. 51 (7) (2003) 1941–1953.
[23] X.-F. Wang, D.S. Huang, A novel density-based clustering framework by using level set method, IEEE Trans. Knowl. Data Eng. 21 (11) (2009) 1515–1531.

Ce Li received his Ph.D. degree in pattern recognition and intelligence system from Xi'an Jiaotong University, China in 2013. He is a professor at the College of Electrical and Information Engineering, Lanzhou University of Technology. His research interests include computer vision and pattern recognition.

Qiang Ma received Bachelor degree in Information and Computing Sciences from Ludong University, China in 2013. He is currently a graduate student in the College of Electrical and Information Engineering in Lanzhou University of Technology. He research interests include digital multimedia forensics and image processing.

Limei Xiao received M.S. degree in computer science from Lanzhou University of Technology, China in 2012. She is currently an assistant professor at the College of Electrical and Information Engineering, Lanzhou University of Technology. Her research interests include image processing and computer software.

Ming Li received Bachelor degree in automation from Lanzhou University of Technology, China in 2011. She is currently a graduate student in the College of Electrical and Information Engineering in Lanzhou University of Technology. Her research interests include scene classification and image processing.

Aihua Zhang received his Ph.D. degree in pattern recognition and intelligence system from Xi'an Jiaotong University, China in 2005. She is a professor at the College of Electrical and Information Engineering, Lanzhou University of Technology. Her research interests include biomedical signal detection, processing and recognition.